AIP | Applied Physics Letters

Towards the development of latent heat storage electrodes for electroporation-based therapies

Christopher B. Arena, Roop L. Mahajan, Marissa Nichole Rylander, and Rafael V. Davalos

Citation: Appl. Phys. Lett. **101**, 083902 (2012); doi: 10.1063/1.4747332
View online: http://dx.doi.org/10.1063/1.4747332
View Table of Contents: http://apl.aip.org/resource/1/APPLAB/v101/i8
Published by the AIP Publishing LLC.

Towards the development of latent heat storage electrodes for electroporation-based therapies

Christopher B. Arena,[1] Roop L. Mahajan,[2] Marissa Nichole Rylander,[3] and Rafael V. Davalos[1,a)]

[1]*Bioelectromechanical Systems Lab, Virginia Tech-Wake Forest School of Biomedical Engineering and Sciences, Virginia Tech, 329 ICTAS Building, (MC0298), Stanger Street, Blacksburg, Virginia 24061, USA*
[2]*Institute for Critical Technology and Applied Science (ICTAS), Virginia Tech, 410H ICTAS Building, (MC0298), Stanger Street, Blacksburg, Virginia 24061, USA*
[3]*Tissue Engineering Nanotechnology and Cancer Research Lab, Virginia Tech-Wake Forest School of Biomedical Engineering and Sciences, Virginia Tech Department of Mechanical Engineering, Virginia Tech, 335 ICTAS Building, (MC0298), Stanger Street, Blacksburg, Virginia 24061, USA*

(Received 24 May 2012; accepted 7 August 2012; published online 22 August 2012)

Phase change materials (PCMs) capable of storing a large amount of heat upon transitioning from the solid-to-liquid state have been widely used in the electronics and construction industries for mitigating temperature development. Here, we show that they are also beneficial for reducing the peak tissue temperature during electroporation-based therapies. A numerical model is developed of irreversible electroporation (IRE) performed with hollow needle electrodes filled with a PCM. Results indicate that this electrode design can be utilized to achieve large ablation volumes while reducing the probability for thermal damage. © *2012 American Institute of Physics*. [http://dx.doi.org/10.1063/1.4747332]

Irreversible electroporation (IRE) is a non-thermal, focal ablation technique invented by Davalos *et al.*[1] that has been translated for the treatment of a variety of cancerous pathologies.[2,3] In a typical surgical procedure, solid metal electrodes are placed directly into a targeted tumor, and a series of short and intense pulsed electric fields (PEFs) are applied. The PEFs cause a migration of charges leading to a rapid increase in transmembrane potential (TMP) across cells comprising the tissue. If the increase in TMP is of sufficient strength and duration, defects are created in the plasma membrane from which the cell cannot recover. The end result is a well-demarcated zone of complete cell death that is visible in real-time on multiple imaging platforms.[4]

The IRE induced lesion volume can be predicted based on the electric field distribution in the tissue.[5] This facilitates the construction of patient specific treatment plans designed around the target tissue's electrical and physiological response to permeabilizing PEFs. Another documented benefit of IRE, which stems from its non-thermal nature, includes sparing of extracellular matrix components, such as major nerve[6] and blood vessel[7] architecture. This enables the treatment of tumors located in close proximity to these sensitive structures that are not candidates for surgical resection[8,9] and promotes rapid lesion resolution within two weeks following treatment.[4]

To capitalize on the benefits of non-thermal ablation, energy delivery is limited to levels that minimize the potential for thermal damage. This restricts the range of applicable parameters to approximately 100 total pulses delivered at a rate of 1 Hz, amplitude of 1000 to 2000 V/cm, and duration of 50 to 100 μs. When large lesions are desired and protocols are selected towards the upper end of this parameter space, there exists a narrow region of tissue adjacent to electrode edges that has a high probability of experiencing thermal damage.[10,11] *We hypothesize that by incorporating phase change materials (PCMs) into the design of electrodes, the peak tissue temperature reached during IRE therapy will be reduced*. Due to their high latent heat of fusion, PCMs absorb heat from the environment during the solid (*s*)–liquid (*l*) transition. This effectively slows the rate of temperature increase. Therefore, these electrodes have the capacity to treat large volumes without any added potential for thermal damage. Here, we model this phenomenon using a numerical implementation of the effective heat capacity method in combination with a model for IRE in liver tissue. Results indicate that the inclusion of a PCM, which melts during treatment, can in fact moderate temperature development within the tissue.

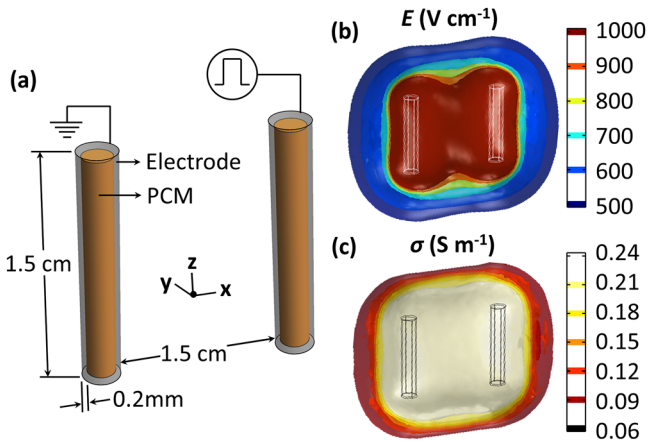

FIG. 1. (a) Schematic diagram of the geometry under consideration with PCM core electrodes used to perform IRE of liver tissue. (b) Electric field distribution resulting from the application of 3000 V to the energized electrode. (c) Electric conductivity distribution resulting from the application of 3000 V to the energized electrode. A non-linear increase in bulk electric conductivity occurs in regions of liver tissue subject to a critical electric field for inducing electroporation. The electrode radius illustrated here is 1.5 mm.

a)Author to whom correspondence should be addressed. Electronic mail: davalos@vt.edu. Telephone: 1-540-231-1979. Fax: 1-540-541-8320.

A 3D finite element model was developed using COMSOL MULTIPHYSICS 4.2a (Stockholm, Sweden) for calculating the electric field and temperature distributions throughout an IRE procedure performed with needle electrodes (Fig. 1). The core material was varied between a salt hydrate PCM (disodium hydrogen phosphate dodecahydrate) and a solid metal equivalent to the electrode shell. A salt hydrate PCM was chosen as this material class has a relatively high thermal conductivity and latent heat of fusion per unit volume compared to organic PCMs,[12,13] which facilitates a rapid phase change with maximum heat absorption. Additionally, many salt hydrates exist with melting points slightly above body temperature. This ensures that the phase transition and subsequent heat absorption begins near the onset of the pulsing sequence.

In the effective heat capacity method, the *s–l* transition is accounted for by including the latent heat of fusion, λ (265.6 kJ kg^{-1})[14] in the volume average of the specific heat capacity at constant pressure

$$c_{p,eq} = \Theta(c_{p,s} + \lambda\Pi) + (1-\Theta)(c_{p,l} + \lambda\Pi), \tag{1}$$

where Θ is the volume fraction of solid material defined by $1 - flc2hs((T\text{-}T_T), R_T)$, and T_T is the transition temperature (40 °C) (Ref. 12) over the transition range, R_T (1 °C). This approximates the logical step $\Theta = 1$ for $T < T_T$ and $\Theta = 0$ for $T > T_T$ by smoothing the transition within the interval $T_T - R_T < T < T_T + R_T$ using a continuous second derivative. Similarly, the term Π is a normalized pulse around the transition temperature defined by $\partial(flc2hs((T\text{-}T_T), R_T))/\partial T$. Smoothing is required for the solver to handle step changes.[15,16] In the PCM domain, the temperature, T, distribution was solved using a modified heat conduction equation, which includes Joule heating, Q_J, due to the application of PEFs

$$\rho_{eq} c_{p,eq} \frac{\partial T}{\partial t} = \nabla \cdot (k_{eq} \nabla T) + Q_J, \tag{2}$$

where ρ_{eq} and k_{eq} are volume averages of the density and thermal conductivity, respectively (Table I)

$$\rho_{eq} = \Theta\rho_s + (1-\Theta)\rho_l \tag{3}$$

and

$$k_{eq} = \Theta k_s + (1-\Theta)k_l. \tag{4}$$

The electrode shell was modeled as stainless steel (AISI 4340) according to the COMSOL material library without any *s–l* transition. In the tissue domain, additional terms accounting for blood perfusion, ω_b, and metabolic heat generation, Q_m, were included in the formulation (Table II)

TABLE I. PCM properties.

Property	Value	Ref.
k [W m^{-1} K^{-1}] (*s*/*l*)	1.0/0.6	14
c_p [J kg^{-1} K^{-1}] (*s*/*l*)	1960/3430	14
ρ [kg m^{-3}] (*s*/*l*)	1520/1450	14
σ [S m^{-1}]	1	—

TABLE II. Tissue properties.

Property	Value	Ref.
k [W m^{-1} K^{-1}]	0.502	19
c_p [J kg^{-1} K^{-1}]	3600	19
ρ [kg m^{-3}]	1060	19
ω_b [1 s^{-1}]	0.0064	19
c_b [J kg^{-1} K^{-1}]	4180	19
ρ_b [kg m^{-3}]	1000	19
Q_m [W m^{-3}]	33 800	26
σ_o [S m^{-1}]	0.067	17

$$\rho c_p \frac{\partial T}{\partial t} = \nabla \cdot (k\nabla T) + \rho_b c_b \omega_b (T_b - T) + Q_m + Q_J. \tag{5}$$

The Joule heating term

$$Q_J = \sigma |E|^2 \tag{6}$$

was obtained by first solving for the electric field, E, distribution in the tissue under the electro-quasistatic approximation

$$-\nabla \cdot (\sigma(|E|)\nabla\Phi) = 0, \tag{7}$$

where Φ is the electric potential and $\sigma(|E|)$ is the dynamic electric conductivity. Equation (7) is valid on the basis that the duration of a constant voltage IRE pulse greatly outweighs the pulse rise/fall time and lends itself to a steady-state approximation. The dynamic electric conductivity function describes how the tissue conductivity changes with electric field due to electroporation. It was constructed by approximating data on electroporation of liver tissue[17] with a smoothed step function $\sigma_o(1 + 2.597 \times flc2hs((E\text{-}T_E), R_E))$, where T_E (650 V/cm) is the location of electric field transition over the range, R_E (150 V/cm). In the electrode and PCM domains, no conductivity dependence on electric field was included in Eq. (7).

Electric potential boundary conditions of 3000 V and 0 V were applied along the outer surfaces of the energized and grounded electrode shells, respectively, and the initial tissue temperature and blood temperature were set to 37 °C. All remaining inner boundaries were treated as continuity, and the outer boundaries were treated as electrically and thermally insulating. The tissue was modeled as a cube (10 cm), and the electrode edge-to-edge spacing (1.5 cm) and height (1.5 cm) were held constant.

A parametric study was performed on electrode radius (0.5 mm to 1.5 mm) in order to investigate a range of sizes that could mitigate temperature increase. A finer, free tetrahedral mesh was used, which resulted in between 145 495 and 188 916 elements, depending on the electrode radius under investigation, and less than 0.1% difference in temperature calculations at the electrode-tissue interface upon successive refinements. Additionally, strict time stepping at 1 s intervals was implemented, as the solver could take additional time steps if necessary to accurately resolve the phase transition. The time of pulsing was 70 s, and the Joule heating term was scaled by the duty cycle (90×10^{-6}) in order to simulate the delivery of 90 μs long pulses at a repetition rate

of 1 Hz. This protocol was chosen based on experimental evidence of thermal damage surrounding solid metal electrodes.[10,11]

The stationary electric field distribution and electric conductivity distribution are shown in Fig. 1 for an electrode radius of 1.5 mm. These results are independent of the electrode core material, as the electric field is zero in those regions. According to the dynamic conductivity function, any tissue exposed to an electric field greater than 700 V/cm is subject to undergo IRE, and any tissue exposed to an electric field greater than 800 V/cm reaches a plateau in conductivity of 0.241 S/m.

The time-course of PCM melting is shown in Fig. 2. Due to symmetry, only a single electrode from the pair is shown at each time step. The *s–l* transition time depends on the PCM volume and electrode radius. Transition time increases as electrode radius increases, due to the greater volume of PCM that must surpass the melting temperature. For an electrode with a 1 mm radius, the phase transition is complete after 55 s. The center portions of the electrodes are the last to melt. As mentioned, the electric field is zero within the electrode core. Therefore, heat is transferred from the surrounding tissue through the electrode shell. Due to the sharp edges at the top and bottom of the electrodes, the electric field is highest in these regions. As a result, the PCM melts preferentially at the top and bottom of the electrodes.

Incorporating PCMs into electrode designs can limit the peak temperature reached during IRE therapy. The effect is highly dependent upon the PCM transition time and the time of pulsing. Fig. 3 shows a plot of temperature versus time at a point at the center of the electrode-tissue interface for a solid metal electrode (Fig. 3(a)) and a PCM core electrode (Fig. 3(b)) of varying radius. In the case of the solid metal electrode, temperature increases sharply during treatment. Additionally, as the radius increases, the maximum temperature reached during treatment decreases. This is due to a decrease in the electric potential gradient surrounding the electrode with increasing radius. In the case of the PCM core electrode, there is a minimal increase in temperature during the phase transition. However, once the PCM is completely melted, the temperature increases at a faster rate and

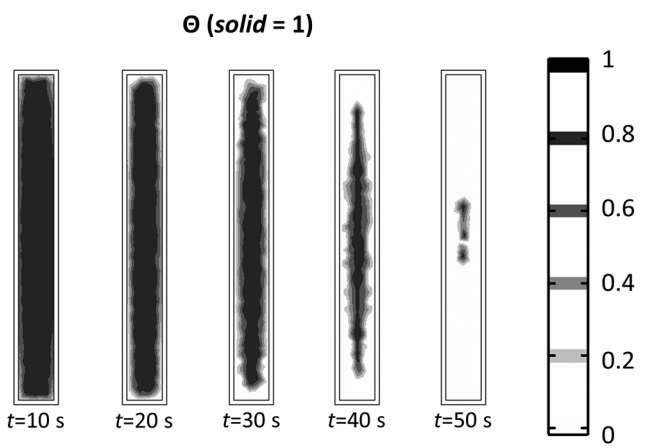

FIG. 2. Time-lapse of the *s–l* transition. For an electrode with a radius of 1.0 mm, the PCM melting process is complete after 55 s. The transition times for the electrode radii not shown (0.5 mm, 0.75 mm, 1.25 mm, and 1.5 mm) are 13 s, 33 s, 76 s, and 104 s, respectively.

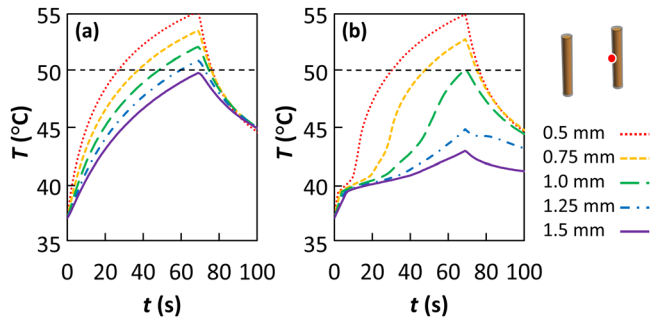

FIG. 3. Temperature development at the center point along the electrode-tissue interface (0.75 cm, 0, 0) for a solid metal electrode (a) and PCM core electrode (b). The IRE treatment consists of 70, 90 μs long pulses applied at a frequency of 1 Hz and voltage-to-distance ratio of 2000 V/cm. The dashed line at 50 °C indicates a threshold for a dramatic increase in the rate of thermal damage.

approaches the temperature of the solid metal electrode. For the 70 pulse protocol, a PCM core electrode with a radius greater than or equal to 1.25 mm ensures that the phase transition is not complete by the end of treatment. As a result, the peak temperature at the electrode-tissue interface is well below the level for accelerated thermal damage (taken here to be 50 °C (Ref. 18)). The results are also dependent upon the applied voltage. Lowering the applied voltage from 3000 V extends the transition time for a given electrode radius due to a reduced heating rate (data not shown).

During the phase transition, the presence of the PCM has the greatest influence on temperatures within and adjacent to the electrodes. Fig. 4 shows the temperature distribution at the end of treatment along a cut line through the center of solid metal electrodes (Fig. 4(a)) and PCM core electrodes (Fig. 4(b)) of varying radius. Between the electrodes, the temperature is also reduced, *albeit* to a lesser degree.

Based on the temperature profiles shown in Fig. 3, the extent of thermal damage at the electrode-tissue interface was quantified using the Arrhenius equation

$$\Omega(t) = \int \zeta e^{-E_a/(RT(t))} dt, \tag{8}$$

where $\Omega(t)$ is the damage integral, ζ is the frequency factor, E_a is the activation energy, R is the universal gas constant, and $T(t)$ is the temperature at a given time, t. These

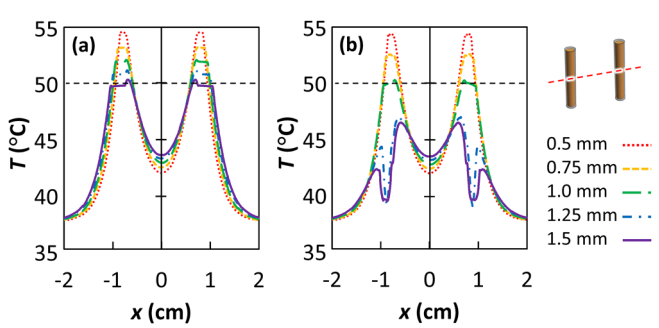

FIG. 4. Temperature cross-section at the end of treatment (t = 70 s) through the center of solid metal electrodes (a) and PCM core electrodes (b). The IRE treatment consists of 70, 90 μs long pulses applied at a frequency of 1 Hz and voltage-to-distance ratio of 2000 V/cm. The dashed line at 50 °C indicates a threshold for a dramatic increase in the rate of thermal damage.

TABLE III. Damage integral, Ω.

Radius (mm)	Solid metal core	PCM core
0.50	2.58	2.33
0.75	1.73	1.25
1.00	1.26	0.62
1.25	0.99	0.30
1.50	0.80	0.21

parameters have been defined for protein coagulation in liver ($E_a = 2.577 \times 10^5$ J mol^{-1} and $\zeta = 7.39 \times 10^{39}$ s^{-1}),[19] where $\Omega = 1$ empirically marks tissue whitening.[20] Equation (8) was solved in WOLFRAM MATHEMATICA 8.0 (Champaign, IL, USA) until the 200 s time point (130 s after the offset of pulsing). For the prescribed treatment, the results indicate that the PCM core reduces the probability of thermal damage in all cases (Table III). The PCM core also has the potential to eliminate tissue whitening seen in IRE with solid metal cores[10,11] if the electrode radius is greater than or equal to 1.0 mm. While larger electrodes are beneficial in terms of reducing thermal damage, they are also associated with increased invasiveness. However, a 1.0 mm radius is typical of liver biopsy needles.[21]

This feasibility study was designed to isolate the effect of the *s–l* transition. To simplify the initial analysis, we have neglected the influence of temperature on electric conductivity. This will likely effect the transition time and be required for experimental validation. Additionally, the dynamic electric conductivity function was modeled after data from rabbit liver, and it will be useful to investigate the influence of other species and organ types on the transition time. Electrodes were approximated as cylindrical shells within a tissue domain large enough to avoid boundary effects. Future work should include the influence of fins and convective cooling along with alternate electrode designs. For instance, plate electrodes used for transdermal applications of electroporation may also benefit from the incorporation of PCMs. The skin is highly resistive and often subject to temperatures above the threshold for thermal damage when exposed to PEFs.[22] An added benefit of plate electrodes is that they are placed externally on the surface of the tissue, and their dimensions can be increased if needed to optimize the PCM transition time without increasing electrode invasiveness.

Alternative methods for reducing thermal damage at the electrode-tissue interface have been proposed. For example, electrodes can be aggressively pre-cooled prior to applying the pulses.[22] However, this requires modifications to surgical procedures and may be difficult to perform with needle electrodes where electrode placement requires extended periods of time, during which the electrodes can equilibrate with their surrounding environment. Active cooling throughout treatment has also been suggested but requires external equipment.

PCMs have been widely used for managing temperature changes in electronics and industrial applications.[15,23–25] Here, we show that they may also have unique benefits when applied to electrode designs for electroporation-based therapies. Specifically, electrodes containing a salt hydrate that transitions from solid-to-liquid during treatment can reduce the peak tissue temperature. This warrants further investigations into alternative materials, including biocompatible PCMs, and electrode designs in order to maximize the reduction in thermal damage for a desired set of pulse parameters.

This work was supported by the NSF (CBET-0933335) and ICTAS Multi-scale Bio-Engineered Devices and Systems (MBEDS) center. The authors thank Michael B. Sano and Paulo A. Garcia for their assistance with developing the numerical models.

[1]R. V. Davalos, L. M. Mir, and B. Rubinsky, Ann. Biomed. Eng. **33**(2), 223–31 (2005).
[2]S. Bagla and D. Papadouris, J. Vascular Int. Radiol. **23**(1), 142–145 (2012).
[3]K. R. Thomson, W. Cheung, S. J. Ellis, D. Federman, H. Kavnoudias, D. Loader-Oliver, S. Roberts, P. Evans, C. Ball, and A. Haydon, J. Vascular Int. Radiol. **22**(5), 611–621 (2011).
[4]B. Rubinsky, G. Onik, and P. Mikus, Technol. Cancer Res. Treat **6**(1), 37–48 (2007).
[5]J. F. Edd, L. Horowitz, R. V. Davalos, L. M. Mir, and B. Rubinsky, IEEE Trans Biomed. Eng. **53**(7), 1409–1415 (2006).
[6]W. Li, Q. Y. Fan, Z. W. Ji, X. C. Qiu, and Z. Li, Plos One **6**(4), e18831 (2011).
[7]E. Maor, A. Ivorra, J. Leor, and B. Rubinsky, Technol. Cancer Res. Treat **6**(4), 307–312 (2007).
[8]P. A. Garcia, T. Pancotto, J. H. Rossmeisl, N. Henao-Guerrero, N. R. Gustafson, G. B. Daniel, J. L. Robertson, T. L. Ellis, and R. V. Davalos, Technol. Cancer Res. Treatment **10**(1), 73–83 (2011).
[9]R. E. Neal II, J. H. Rossmeisl, Jr., P. A. Garcia, O. I. Lanz, N. Henao-Guerrero, and R. V. Davalos, J. Clin. Oncol. **29**, e372 (2011).
[10]E. Ben-David, L. Appelbaum, J. Sosna, I. Nissenbaum, and S. N. Goldberg, Am. J. Roentgenol. **198**(1), W62–W68 (2012).
[11]L. Appelbaum, E. Ben-David, J. Sosna, Y. Nissenbaum, and S. N. Goldberg, Radiology **262**(1), 117–125 (2012).
[12]A. Sharma, V. V. Tyagi, C. R. Chen, and D. Buddhi, Renewable Sustainable Energy Rev. **13**(2), 318–345 (2009).
[13]M. F. Demirbas, Energy Sources Part B **1**(1), 85–95 (2006).
[14]S. Hirano, T. S. Saitoh, M. Oya, and M. Yamazaki "Long-term supercooled thermal energy storage (thermophysical properties of disodium hydrogenphosphate $12H_2O$)," in Energy Conversion Engineering Conference and Exhibit, 2000. (IECEC) 35th Intersociety [IEEE, **2**, 1013–1018 (2000)].
[15]S. Krishnan and S. V. Garimella, IEEE Trans. Compon. Packag. Technol. **27**(1), 191–199 (2004).
[16]J. A. Dantzig, Int. J. Numer. Methods Eng. **28**(8), 1769–1785 (1989).
[17]D. Sel, D. Cukjati, D. Batiuskaite, T. Slivnik, L. M. Mir, and D. Miklavcic, IEEE Trans. Biomed. Eng. **52**(5), 816–827 (2005).
[18]R. V. Davalos, B. Rubinsky, and L. M. Lir, Bioelectrochemistry **61**(1–2), 99–107 (2003).
[19]I. A. Chang and U. D. Nguyen, Biomed. Eng. Online **3**(1), 27 (2004).
[20]K. Beop-Min, S. L. Jacques, S. Rastegar, S. Thomsen, and M. Motamedi, IEEE J. Sel. Top. Quantum Electron. **2**(4), 922–933 (1996).
[21]E. R. Littlewood, I. T. Gilmore, I. M. Murraylyon, K. R. Stephens, and F. J. Paradinas, J. Clin. Pathol. **35**(7), 761–763 (1982).
[22]S. M. Becker and A. V. Kuznetsov, Int. J. Heat Mass Transfer **50**(1–2), 105–116 (2007).
[23]A. Abhat, Sol. Energy **30**(4), 313–332 (1983).
[24]A. M. Khudhair and M. M. Farid, Energy Convers. Manage. **45**(2), 263–275 (2004).
[25]B. Zalba, J. M. Marin, L. F. Cabeza, and H. Mehling, Appl. Thermal Eng. **23**(3), 251–283 (2003).
[26]P. Keangin, P. Rattanadecho, and T. Wessapan, Int. Commun. Heat and Mass Transfer **38**(6), 757–766 (2011).